ACS OMEGA

http://pubs.acs.org/journal/acsodf

Article

Removal of As(V) and Cr(VI) with Low-Cost Novel Virgin and Iron-Impregnated Banana Peduncle-Activated Carbons

Zobia Razzaq, Muhammad Hamayun,* Shahzad Murtaza, Samia Kausar, Ataf Ali Altaf,* Rizwan Ullah Khan, and Tehzeen Javaid

Cite This: *ACS Omega* 2023, 8, 2098−2111

Read Online

ACCESS | Metrics & More | Article Recommendations | Supporting Information

ABSTRACT: This work reports the investigation of activated carbons from virgin banana peduncle (**ZR1**) and iron-impregnated banana peduncle (**ZR2**) as adsorbents for the removal of As(V) and Cr(VI) ions from aqueous solutions. Both adsorbents were characterized through the point of zero charge, powder X-ray diffraction, scanning electron microscopy, energy-dispersive X-ray, Brunauer−Emmett−Teller, and Fourier transform infrared spectroscopic techniques. The effects of initial pH, contact time, temperature, and initial concentration on metal ion adsorption were investigated. Adsorbents existed as both crystalline and amorphous species having homogeneous surface cavities and surface area of 749.73 and 369.66 m^2/g for **ZR1** and **ZR2**, respectively. The maximum As(V) removal of 79.32 and 69.08% was obtained using **ZR1** and **ZR2**, respectively, whereas the maximum Cr(VI) removal was calculated as 69.73% for **ZR1** and 73.78% for **ZR2**. Kinetic modeling data were found to be best fitted for the pseudo-second-order reaction, and rate constants were calculated. The theoretical adsorption capacities (q_m) of **ZR1** and **ZR2** were calculated through Langmuir and Freundlich models. The maximum As(V) adsorption capacities calculated for **ZR1** and **ZR2** were 13.33 and 9.066 mg/g, respectively, whereas the maximum Cr(VI) adsorption capacity for both was 13.26 mg/g at 298−328 K. The reaction was endothermic with decreased randomness at the solid−liquid interface due to positive entropy and enthalpy values. All kinetic and thermodynamic parameters showed the feasibility of the adsorption process, and characterization after adsorption indicated **ZR1** and **ZR2** novel activated carbons as efficient and cheapest biosorbents for removing As(V) and Cr(VI).

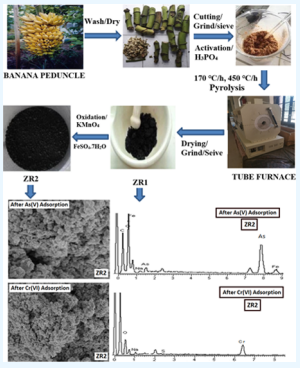

1. INTRODUCTION

Today, environmental pollution and global warming are major concerns due to heavy metal contamination. These heavy metals and their related compounds are injurious and harmful to human health. Some heavy metals are necessary for life in very small amounts; however, when inhaled in large amounts, they are toxic and injurious. Different metals like chromium (Cr), arsenic (As), copper (Cu), lead (Pb), mercury (Hg), cadmium (Cd), and zinc (Zn) contaminate water. Human activities causing air, water, and soil pollution are the natural, geological and biological sources of heavy metal production and spread.[1]

Arsenic (As), a metalloid, is known as a poisonous element and very toxic to humans. Arsenic has been mostly found as arsenate As(V) and arsenite As(III), which are produced by different natural sources, such as weathering reactions and biological activities, and are the main reason for the contamination of arsenic in different manufacturing units.[2] Arsenic(V) has received more attention due to its easy removal compared to arsenite(III), which cannot be removed directly; it is first converted into As(V) and then removed from the water. The health hazards caused by the long-term uptake of arsenic(V)-contaminated water can cause peripheral neuropathy, peripheral vascular diseases, dermal liaisons, anhydremia, hematopoietic depression, portal cirrhosis, and ascites, loss of weight, anorexia and sensory disturbance, peripheral neuritis, diarrhea, vomiting, and abdominal and esophageal pain.[3]

Chromium(VI) is another important heavy metal that exists in several oxidation states in the aquatic environment.[4] It has been found in the air, water, and soil in the forms of Cr(III) and Cr(VI), which are produced during chrome plating, formation of dyes and pigments, leather tanning, and wood preserving applications.[5] In the air, chromium compounds are present mostly as fine dust particles, which eventually settle over land and water, and the concentration of chromium in the surface water is found to be 1−10 μg/L. Cr(VI) compounds have received more attention due to their versatile properties such as high water solubility, mobility, nonbiodegradability, toxicity, mutagenicity, and carcinogenicity compared to Cr(III) compounds.[6] Inhalation of large concentrations of Cr(VI) can cause different diseases such as irritation to the nose, runny nose, nose bleeds, ulcers, and holes in the nasal septum.

Received: September 14, 2022
Accepted: December 22, 2022
Published: January 9, 2023

ACS Publications

© 2023 The Authors. Published by American Chemical Society

Scheme 1. Synthetic Scheme for ZR1 and ZR2

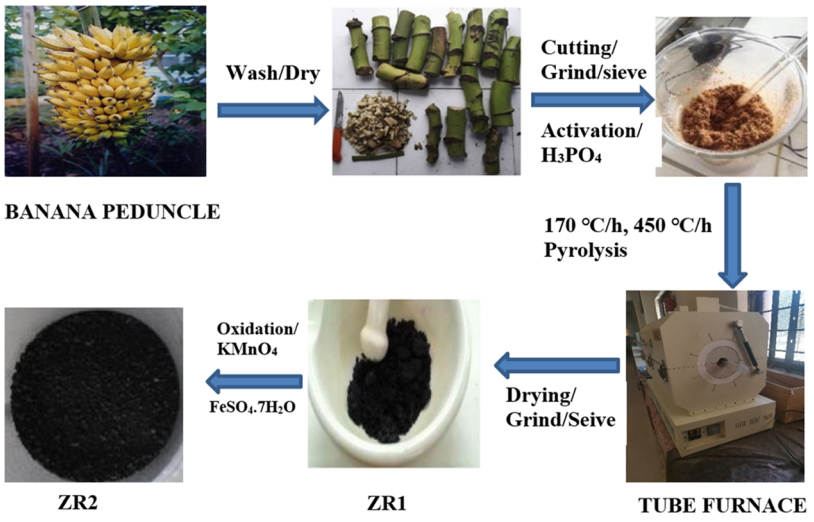

Ingestion of Cr(VI) can induce stomach and skin ulcers, convulsions, kidney and liver damage, lung cancer, and even death.[7]

There are several conventional methods for removing heavy metals from water, which include precipitation, ion exchange, reverse osmosis, electrocoagulation, and nanofiltration but the most efficient and economic method is adsorption due to low cost and simplicity.[8] However, these methods are limited for the use of large industries, since the operational cost is high. Among these technologies, adsorption is the most favorable technology in screening the various contaminants from the aqueous system because the system is cost-effective, easy to handle, free of sludge production, and versatile.[9]

Many adsorbents have been reported for the removal of pentavalent arsenic and hexavalent chromium from water such as activated carbons (AC), activated alumina, chitosan polymer, zeolite, low-cost bioadsorbents such as olive, leaves, wool, etc., sawdust, rice husk, wheat bran, bentonite, metal oxides such as ferric hydroxide, ion exchange resin, nano-structured adsorbents, etc.[10] Mostly nanoporous and nano-structured materials have a unique surface area and structural and bulk properties. Due to these properties, nanomaterials have important applications in environmental remediation and water purification.[11] Globally, activated carbon and resins of ion exchange have been widely used for adsorption and found to be less utilized in developing countries due to their high cost and operational complexities.[12] Additionally, converting the agricultural byproducts into activated carbon could hypothetically be helpful for environmental preservation by making the emissions produced by landfilling and ignition of organic materials very low.[13]

Banana, being an annual crop, is cultivated to produce nearly 220 t/hectare. Mostly available abundantly plant residual wastes which mainly consist of lignocellulose material. Banana peduncles (BPs) have been produced from banana plants, which act as an important low-cost adsorbent for heavy metals, especially for As(V) and Cr(VI) removal from water.[14] Previous research had worked on different parts of banana plants, i.e., shells, trunks, stems, leaves, and core, for the removal of heavy metals from contaminated water.[15] The present study reports indigenously synthesized virgin (**ZR1**) and iron-impregnated (**ZR2**) banana peduncle as low-cost activated carbon-based adsorbents. Both adsorbents are characterized and investigated for the adsorptive removal of As(V) and Cr(VI).

2. EXPERIMENTAL SECTION

2.1. Materials and Methods. $KMnO_4$, $K_2Cr_2O_7$, H_3PO_4, and $FeSO_4{\cdot}7H_2O$ were used in this study. All of the chemicals were of analytical grade and purchased from Sigma-Aldrich.

The point of zero charge (PZC) of **ZR1** and **ZR2** was determined by a 0.1 M sodium chloride solution. The pH of the solution was varied from 4 to 12 using 0.1 M HCl/NaOH solutions. Powder X-ray diffraction (PXRD) measurements were performed by an X-ray diffractometer (Bruker, AXS D8; Yokohama-shi, Japan) with Cu Kα radiation (1.5406 Å). The morphological features of the banana peduncle were characterized by a scanning electron microscope (SEM, JEOL, JSM-6360 EO; Tokyo, Japan), and the elemental composition was estimated by an energy-dispersive X-ray (EDX) diffractometer (JEOL JSM-6360 LV; Tokyo, Japan). The surface area and pore structure parameters were calculated by Brunauer−Emmett−Teller (BET) analysis performed using a Quantachrome Nova 2200e (Tokyo, Japan). A sonicator (Bransonic 2510EMT bath; Darmstadt, Germany) was used for the surface area determination of nanomaterials. Fourier transform infrared (FTIR) analysis was performed by an IR Prestige-21 FTIR-84005 (Merck, Darmstadt, Germany), SHIMADZU Corporation, which was utilized to confirm the presence of functional groups on the surface of activated carbons.

2.2. Raw Material and Processing of Banana Peduncle. The raw material of banana bunches called banana peduncles was collected from different areas of Barnala city of Azad Kashmir, Pakistan. Banana peduncle (BP) is one of the cheapest biomass sources that are abundantly available in the market of Pakistan and has been used for the preparation of activated biosorbents for the removal of As(V) and Cr(VI) from the aqueous phase. Banana peduncles were washed with fresh tap water and then with double distilled water. After washing, banana peduncles were cut and dried in sunlight for one month. The dried banana peduncles were first ground by hand in a mortar and pestle and then in a blender and finally sieved through a 250 μm sieve. Finely ground banana peduncles were further dried at 200 °C for 2−3 h and stored in the bottle for further studies.

https://doi.org/10.1021/acsomega.2c05957
ACS Omega 2023, 8, 2098−2111

2.3. Synthesis of Activated Carbons. Activated carbons **ZR1** and **ZR2** were prepared from banana peduncle by a literature-reported two-step pyrolysis method and are depicted in Scheme 1.[16] **ZR1** was prepared by mixing an activating agent [a 50% w/v solution of H_3PO_4] with the raw material of banana peduncle (100 g) in 1:1 by weight and heated at 170 °C/h (±5 °C) and 450 °C/h (±5 °C) in a tube furnace. Further, after the heat treatment, the synthesized material was subjected to cooling by washing it with deionized water and drying it in sunlight for one day. Further drying was carried out in an oven at 110 °C for 2−3 h. After drying, **ZR1** was ground and sieved to store for further studies.

The iron-impregnated banana peduncle (**ZR2**) was prepared by impregnation of 50 g of virgin activated carbon (**ZR1**) oxidized with a 10% solution of potassium permanganate [$KMnO_4$] and then iron metal-impregnated by treatment with 4.96 g of ferrous sulfate [$FeSO_4{\cdot}7H_2O$] solution. First, carbon was mixed with different concentrations of $KMnO_4$ solution and stirred for 20 min. The pH was noted before and after stirring the sample. After stirring, the sample was washed with deionized water, till the disappearance of pinkish color. In the second step, iron loading was done by treating the sample with various concentrations of the $FeSO_4{\cdot}7H_2O$ solution, and the mixture was stirred for 8 h. The pH was noted before and after stirring the mixture. After stirring, the sample was washed and soaked overnight with a 1% $NaHCO_3$ solution. After soaking, the sample was washed with deionized water, filtered, and dried at 110 °C for further use.

2.4. Adsorption Activity. *2.4.1. Solution Preparation.* The stock solution of $K_2Cr_2O_7$ was prepared by dissolving 2.83 g of it into little deionized water in a 1000 mL flask. Dilution solutions having 30, 50, 70, 90, and 110 mg/L concentrations were prepared by adding 2.5, 7.5, 12.5, 17.5, 22.5, and 27.5 mL, respectively, of the stock solution into a 250 mL flask. The solution of 50 mg/L was used as a working solution for activity.

2.4.2. Adsorptive Removal of As(V) and Cr(VI). The batch adsorption was carried out to investigate the effect of different parameters such as pH, contact time, and temperature on the uptake of As(V) and Cr(VI) by 0.1 g of **ZR1** and **ZR2**. The percentage removal was calculated by the following equation:[17]

$$\%\ \text{removal} = \frac{(C_i - C_f)}{C_i} \times 100 \quad (1)$$

The adsorptive removal of As(V) and Cr(VI) using **ZR1** and **ZR2** biosorbents was investigated at different pH values, i.e., 2, 4, 6, 8, and 10. For the activity, 0.05 g of **ZR1** and **ZR2** adsorbents were taken in a series of 250 mL flasks each containing 40 mL of 50 mg/L solutions of adsorbates. For 4 h, the suspensions were dazed in a thermostat shaker bath at 25 °C. After shaking the solutions, they were filtered and their final pH values were noted. Also, adsorption concentrations were measured by an atomic absorption spectrophotometer (Analyst 800), and the final concentrations of As(V) and Cr(VI) ions in the solutions were determined. The test solutions' pH was maintained by adding reagent-grade diluted (0.1 M) hydrochloric acid and (0.1 M) sodium hydroxide solution.

The adsorption activity was also investigated through the same method described above at different contact times, i.e., 5, 10, 20, 30, 45, 60, 90, 120, 150, and 180 min, and temperatures, i.e., 298, 308, 318, and 328 K, using different adsorbate solution concentrations, i.e., 30, 50,70, 90 and 110 mg/L. Onto the solid surface of the adsorbent, the amounts of As(V) and Cr(VI) adsorbed (q_e) in mol/g were calculated from their C_f (equilibrium concentrations) in mol/L at different time intervals (t) by eq 2.[18]

$$q_e = \frac{(C_i - C_f) \times V}{W \times 1000} \quad (2)$$

where C_i and C_f are the initial and equilibrium concentrations (mg/L) of arsenate (V) and Cr(VI) in solutions, respectively, W is the weight of the dry adsorbent in grams, and V is the volume (mL) of the adsorbent.

2.4.3. Investigation of Kinetic and Thermodynamic Parameters. The pseudo-first-order and pseudo-second-order kinetic models were applied to the experimental data of the adsorption process to evaluate the correlation and the feasibility of the adsorption reaction.[19] The Langmuir−Freundlich isotherm applied to the experimental data obtained for both **ZR1** and **ZR2** as catalysts in adsorption activity. A thermodynamic study was carried out in 100 mL conical flasks with 40 mL of 50 mg/L solutions of Cr(VI) and As(V) separately in each flask for the adsorption isotherm at different concentrations (30, 50, 70, 90, and 110 mg/L), temperatures (298−328 K), and pH values (2−10). Thermodynamic parameters such as enthalpy, entropy, and Gibbs free energy were calculated separately for As(V) and Cr(VI) uptake onto **ZR1** and **ZR2** using Gibbs free energy and the van't Hoff plot. The separation parameters, ΔH, ΔS, and ΔG, have been calculated by the plot of $\ln q_m$ and 1/T.

2.4.4. Desorption Study. Desorption of arsenate and chromate from the laden surface sites of **ZR1** and **ZR2** was studied by adding 0.05 g of the loaded surface of arsenate and chromate into 40 mL of deionized water taken in different polythene bottles. Initially, the pH of the suspensions in the polythene bottles was adjusted from 2 to 10 by the addition of 0.1 M HNO_3/NaOH solutions, which were then agitated for 24 h in a mechanical shaker bath. After shaking the reaction vessels, the final pH of the suspensions was noted and subjected to filtration. The amounts of arsenate and chromate desorbed from the loaded surface of **ZR1** and **ZR2** into filtrates were analyzed by an atomic absorption spectrophotometer.

3. RESULTS AND DISCUSSION

3.1. Characterization of Activated Carbon Adsorbents (ZR1 and ZR2). The synthesized activated carbons were structurally characterized by the point of zero charge (PZC) and powder X-ray diffraction (PXRD) to find out phase composition, scanning electron microscopy (SEM) for surface morphology, energy-dispersive X-ray (EDX) for elemental composition, Brunauer−Emmett−Teller (BET) to find out surface areas and pore characters, and Fourier transform infrared (FTIR) spectroscopic analysis.

3.1.1. Point of Zero Charge (PZC) Analysis. The PZC was calculated to know the acidic and basic nature of the surface of **ZR1** and **ZR2** adsorbents. At PZC, the surface charge becomes neutral corresponding to the state of the solid surface, where the concentrations of hydrogen and hydroxyl ions become equal and the surface is said to have a zero charge. pH_{PZC} was determined by a well-known salt addition method,[20] which was found to be 6 for arsenate and chromate onto **ZR1** and **ZR2** (Figure S1a−d in the Supporting Information). This value of PZC for **ZR1** and **ZR2** was similar to that reported for

https://doi.org/10.1021/acsomega.2c05957
ACS Omega 2023, 8, 2098−2111

activated carbon prepared from *Terminalia chebula*.[21] A point of zero charge test was carried out, which showed that the pH_{PZC} values were 4 and 6 for **ZR1** and **ZR2**, respectively. It has been calculated that below this pH, the adsorbent gets a positive charge, and above this pH, the adsorbent gets a negative charge. But at pH equal to pH_{PZC}, the adsorbent is neutral. The prepared banana peduncles were characterized for PZC by the salt addition procedure, and the results are presented in Figure 1 for arsenate and chromate onto **ZR1** and **ZR2**, respectively.

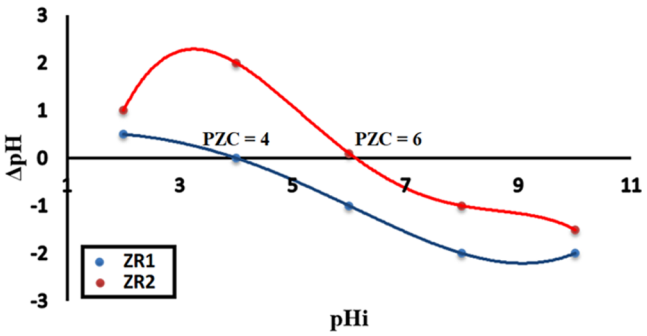

Figure 1. Point of zero charge (PZC) for **ZR1** and **ZR2**.

3.1.2. Powder X-ray Diffraction (PXRD) Analysis. The powder XRD patterns are depicted in Figure 2 for **ZR1** and

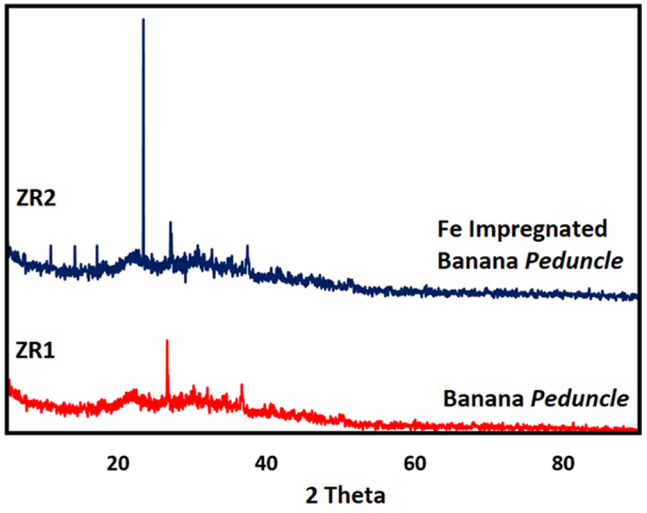

Figure 2. Powder XRD spectra of **ZR1** and **ZR2**.

ZR2 samples having sharp peaks, indicating the noncrystalline nature of the synthesized materials. The powder patterns obtained match the standard powder patterns (JCPDS card 00-003-0569).[22] The sharp peak at the corresponding 26.60 2θ value for **ZR1** and **ZR2** in the PXRD pattern corresponds to the (002) planes of carbon materials,[23] whereas **ZR2** has a sharp signal at the 23.05 2θ value, which is due to Fe impregnation and matches well with the crystalline iron species akaganeite (β-FeOOH).[24] The results of this study found that impregnated iron existed as both crystalline and amorphous species as broad and sharp peaks observed in the PXRD pattern, respectively. Crystallinity increased from **ZR1** to **ZR2** after iron impregnation as the sharpness of peak intensities increased. Also, it is evident from the literature that crystallinity arises in iron-impregnated activated carbons in the temperature range of 600−800 °C.[25]

3.1.3. SEM and EDX Analysis. The SEM photographs of **ZR1** and **ZR2** samples are presented in Figure 3, showing rod-like structures, but more spacing is found in virgin banana peduncle (**ZR1**) compared to iron-impregnated banana peduncle (**ZR2**). The micrographs showed that the surface of **ZR2** carbon was homogeneous. It was observed from SEM micrographs that the external surface of **ZR2** carbon contained cavities that formed as a result of the evaporation of H_3PO_4 during carbonization. However, the cavities of the various carbon samples were not clear, which may be due to the surface modification with iron. EDX analysis of the **ZR1** adsorbent showed characteristic peaks of carbon, which decreased with time due to C−O bond formation, as shown in Figure 3, whereas a sharp characteristic Fe peak was observed for iron-impregnated **ZR2**.

3.1.4. BET Surface Area Analysis. The specific surface areas of the synthesized **ZR1** and **ZR2** activated carbons were evaluated from N_2 adsorption isotherms. Table 1 summarizes the BET surface area (m^2/g), S_{DR}, S_{BJH}, micropore volume, and average pore width of the adsorbents. Both carbon adsorbents in the experimental work had high surface areas (**ZR1**: 749.73 m^2/g and **ZR2**: 369.66 m^2/g). **ZR2** had a lower surface area due to spaces covered by the iron element. The pore volume of **ZR1** (0.455 cm^3/g) was greater than that of **ZR2** (0.322 cm^3/g), and these characters have shown the mesoporous nature of the synthesized activated carbons.

3.1.5. FTIR Analysis. The presence of the functional group on the surface of adsorbents was investigated by FTIR spectroscopy. The FTIR spectra shown in Figure S2 in the Supporting Information showed characteristic peaks for both **ZR1** and **ZR2** activated carbons, which were simple and similar, and the main difference between them was a band around 586 cm^{-1}. This band is attributed to the stretching and torsional vibration of Fe−O bonds. A band in the region of about 1600 cm^{-1} can be observed in all spectra, which is attributed to water molecules bound in various ways. The FTIR spectrum of the banana peduncle shown in Figure 6 has three different adsorption peaks. The peak at 3400−3500 cm^{-1} is attributed to the OH functional group. The adsorption peak band at 1500−1650 cm^{-1} is attributed to the primary amine N−H functional group, the peak band at 2800−2950 cm^{-1} is due to the carboxylic acid (−COOH) group, and the peak band at 1050−1100 cm^{-1} is attributed to the C−O bond. A previous study had shown that hydroxyl and carboxylic groups played a major role in the adsorption process.[22b] According to a previous study, the hydroxyl group has effective potential toward the adsorption rate and is efficient through exchange with metal ions. Meanwhile, the carboxylic acid group has a relatively high adsorption rate due to the presence of more negatively charged groups on its surface.[26] A band at approximately 825 cm^{-1} in the spectrum of iron-impregnated banana peduncle after adsorption can be observed, which is attributed to arsenate. However, in FTIR analysis, the shift in bands and wavelength number and absorbance changes between **ZR1** and **ZR2** presented the chemical modification, which took place during pyrolysis.[27]

3.2. Adsorption of As(V) and Cr(VI) Activity. *3.2.1. Effect of pH.* The effect of pH plays a significant role in the adsorption study, as it greatly influences the interactions between the adsorbent and the adsorbate. The pH effect was carried out by changing of pH to acidic (2,4), neutral (6), and

https://doi.org/10.1021/acsomega.2c05957
ACS Omega 2023, 8, 2098−2111

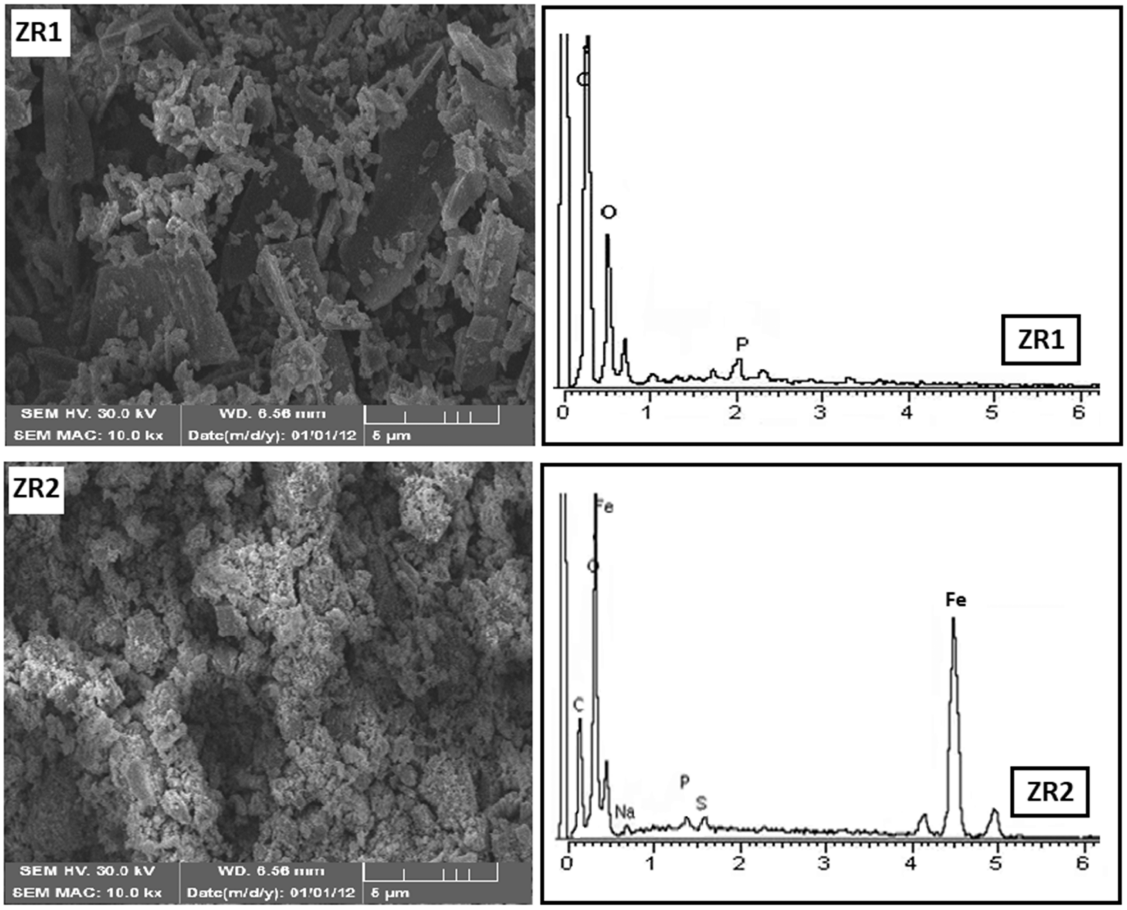

Figure 3. SEM and EDX spectra of **ZR1** and **ZR2**.

Table 1. BET Surface Area Properties of ZR1 and ZR2

properties	ZR1	ZR2
surface area (S_{BET}), m^2/g	749.7	369.7
surface area (DR), m^2	199.7	76.70
average pore width (DR), (Å)	176.5	151.9
adsorption energy (DR), kJ/mol	1.820	1.320
micropore volume (DR), (cm^3/g)	0.741	0.480
micropore surface area (DR), (m^2/g)	299.7	99.88
pore diameter (DA), (Å)	1.92×10^1	1.52×10^1
surface area (BJH), (m^2/g)	749.7	399.7
pore volume (BJH), (cm^3/g)	0.455	0.322

basic (8,10). The amounts (q_e (mg/g)) of As(V) and Cr(VI) adsorbed on the surfaces of **ZR1** and **ZR2** catalysts calculated at different pH values are shown in Figure 4 and enlisted in Table S1 in the Supporting Information. The percentage removal of As(V) and Cr(VI) of **ZR1** and **ZR2** was calculated and is enlisted in Table 2. The results obtained showed that the adsorption is maximum at acidic pH (2−4). At low pH (2−4), the surface of the adsorbent becomes highly protonated, and the maximum adsorbate gets adsorbed on it by the electrostatic force of attraction. Similarly, at high pH (8−10), the adsorption rate becomes very low due to repulsive forces between the adsorbent and the adsorbate. The removal percent was high at acidic pH (2−4), i.e., 86−68%, average at pH 6, i.e., 50−55%, and low at higher pH, i.e., 40−5%, for **ZR1** and **ZR2**. The percentage removal of arsenic and chromium decreased with the increase in pH. The optimum adsorption occurred at pH 4, with maximum As(V) removal capacities of

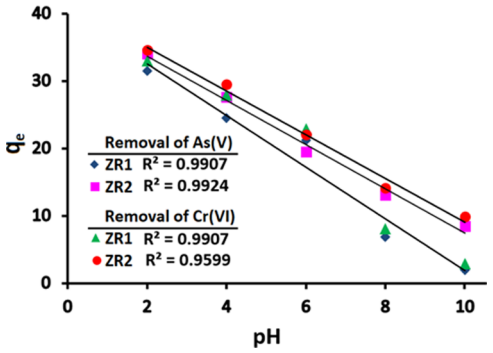

Figure 4. Effect of pH on the removal of 50 mg/L As(V) and Cr(VI) with **ZR1** and **ZR2** at 298 K.

Table 2. Effect of pH on the Removal of As(V) and Cr(VI) with ZR1 and ZR2 at 298 K

	% As(V) removal		% Cr(VI) removal	
pH	ZR1	ZR2	ZR1	ZR2
2	78.68	85.08	82.48	86.48
4	79.32	69.08	69.78	73.78
6	53.02	48.82	57.22	55.22
8	17.08	32.66	20.26	37.20
10	4.90	21.08	7.32	24.66

79.32% for **ZR1** and 69.08% for **ZR2**, whereas the Cr(VI) removal capacity was calculated maximum as 69.73% for **ZR1** and 73.78% for **ZR2** (Table 2).

https://doi.org/10.1021/acsomega.2c05957
ACS Omega 2023, 8, 2098−2111

The decrease in arsenate and chromate uptake with an increase in alkalinity can also be attributed to the point of zero charge. The point of zero charges for **ZR1** and **ZR2** are 4 and 6, respectively (Figure 1), hence below pH_{PZC}, the surface bears a positive charge, whereas above the pH_{PZC} value, the surface is negatively charged. Similarly, arsenate exists as $H_2AsO_4^{-1}$ and $HAsO_4^{-2}$ in the pH range of 5−8.5, and chromate exists as CrO_4^{-2} and $Cr_2O_7^{-2}$. The higher adsorption in the acidic pH range may be attributed to the strong interaction between the negatively charged arsenate and chromate anions and the positively charged surface sites.[28] At the same time, the low adsorption at pH > PZC may be assigned to the repulsive forces between negatively charged arsenate and chromate anions and the negatively charged surface sites. Also, the decrease in adsorption with the increase in pH may be due to the increased competition of OH ions with arsenate and chromate anions for the same adsorption sites of **ZR1** and **ZR2**, respectively.

3.2.2. Contact Time Study. During the adsorption process, contact time plays an important role. For contact time, the study used time intervals of 5, 10, 20, 30, 45, 60, 90, 120, 150, and 180 min. The amounts (q_e) of As(V) and Cr(VI) adsorbed on the surfaces of **ZR1** and **ZR2** catalysts calculated at various contact times are shown in Figure 5 and enlisted in

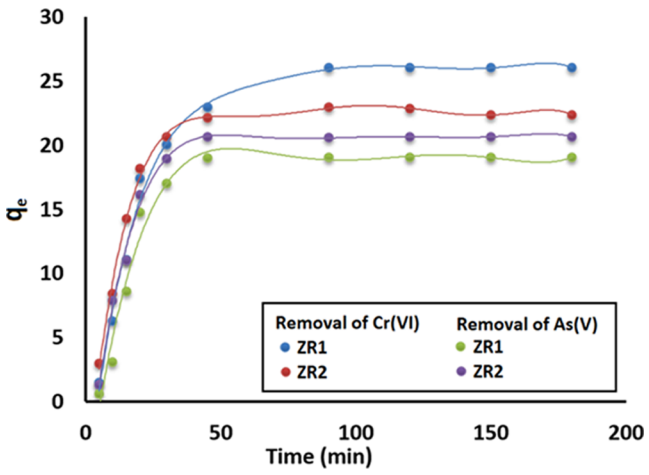

Figure 5. Effect of contact time on the removal of 50 mg/L As(V) and Cr(VI) with **ZR1** and **ZR2** at 298 K.

Table S2 in the Supporting Information. The percentage removal of As(V) and Cr(VI) of **ZR1** and **ZR2** was calculated and is enlisted in Table 3. The results obtained presented that the maximum adsorption was achieved within 1 h (60 min), and after that, the adsorption rate was at equilibrium. The reason is that maximum adsorption sites are available for **ZR1** and **ZR2** adsorbents at the start, but with the passage of time, the available sites become occupied by As(V) and Cr(VI) uptake onto **ZR1** and **ZR2**, resulting in slow adsorption. The removal of As(V) and Cr(VI) increased with the increase of contact time and was maximum at 90 min; after that, the adsorption process slowed down, and equilibrium was achieved with time. At the start of the time interval 5−45 min, removal was 47.50−57.38%; at 90 min, removal was 47.62−61.44%, and at 150−180 min, the removal of arsenic and chromium at equilibrium was 45−55% (Table 3).

3.2.3. Effect of Temperature. The removal of different As(V) and Cr(VI) concentrations, i.e., 30, 50, 70, 90, and 110

Table 3. Effect of Contact Time on the Removal of 50 mg/L As(V) and Cr(VI) with ZR1−ZR2 at 298 K

	% As(V) removal		% Cr(VI) removal	
time (min)	ZR1	ZR2	ZR1	ZR2
5	01.58	03.38	03.78	07.58
10	07.76	15.78	15.76	21.08
15	21.70	27.68	27.70	35.70
20	36.88	42.88	50.20	45.50
30	47.38	47.38	52.00	51.74
45	47.70	51.62	57.38	54.52
90	47.52	51.62	61.52	57.38
120	47.62	51.64	61.44	55.64
150	47.66	51.68	61.68	55.68
180	47.66	51.68	61.68	55.68

mg/L, with **ZR1** and **ZR2** at different temperatures, i.e., 298−328, was investigated and is enlisted in Table 4. The amounts (q_e) of As(V) and Cr(VI) adsorbed on the surface of **ZR1** and **ZR2** catalysts calculated at different temperatures are shown in Figure 6 and enlisted in Table S3 in the Supporting Information. The percentage removal of As(V) and Cr(VI) of **ZR1** and **ZR2** was calculated and is enlisted in Table 4. The adsorption increases initially and then starts to slow down. This gradual change was because of an endothermic reaction, as, initially, the interactions between the adsorbent and the adsorbate increased with increasing temperature, but these interactions no longer remained stronger and started to weaken down. The percentage removal of arsenic and chromium was maximum (60−65%) at higher concentrations (30 mg/L solutions), lower (8.5−15%) at low concentrations (90−110 mg/L solutions), and average (20−40%) at 70 mg/L solutions; with the increase of the concentrations of **ZR1** and **ZR2**, the maximum removal of arsenic and chromium was achieved.

3.3. Evaluation of Kinetic and Thermodynamic Parameters. The kinetic data were plotted according to the pseudo-second-order model, which was found to be best fitted on experimental data (eq 3) plots presented in Figure 7. The linear form of second-order reactions is given below.[29]

$$\frac{t}{q_e} = \frac{1}{k_2 \times q_{e\,2}} + \frac{1}{q_e} \times t \quad (3)$$

Different parameters, i.e., adsorption capacity (q_e) and rate constants (K_2), were calculated from the intercept and slopes of the plots depicted in Figure 7 for As(V) and Cr(VI) uptake and are enlisted in Table 5. However, the investigation of the correlation coefficient, rate constants, and the difference between theoretical and experimental adsorption capacities revealed the higher and best applicability of the pseudo-second-order model. The correlation coefficient (R^2) values were near to unity, giving the basis for this model to best fit to kinetic studies. Besides, the close concurrence between the experimental and calculated values of sorption maxima also decided the best fit of the pseudo-second-order study of As(V) and Cr(VI) onto **ZR1** and **ZR2**.

ZR1 and **ZR2** have shown efficient adsorption capacities for As(V) and C(VI) in comparison to various other literature-reported activated carbon-based adsorbents, which were made by other parts of the banana plant. A comparison of various literature-reported adsorbents with this work was made, as

https://doi.org/10.1021/acsomega.2c05957
ACS Omega 2023, 8, 2098−2111

Table 4. Effect of Different Temperatures on the Removal of Various As(V) and Cr(VI) Concentrations with ZR1−ZR2 at pH 6

	ZR1				ZR2			
	removal of As(V)							
concn (mg/L)	298 K	308 K	318 K	328 K	298 K	308 K	318 K	328 K
30	65.66	62.30	60.16	58.50	65.63	58.96	53.83	50.16
50	39.38	35.38	32.88	31.90	39.38	29.38	24.78	28.78
70	26.27	24.50	22.92	22.35	26.27	20.55	14.84	12.50
90	12.38	12.38	13.57	13.27	12.38	12.45	11.13	10.05
110	09.13	10.86	09.95	08.15	09.13	09.71	08.63	08.10
	ZR1				ZR2			
	removal of Cr(VI)							
concn (mg/L)	298 K	308 K	318 K	328 K	298 K	308 K	318 K	328 K
30	68.30	65.63	65.63	58.16	73.23	69.90	67.83	69.83
50	37.38	35.38	33.38	29.36	41.50	39.50	37.96	38.10
70	24.88	24.24	24.24	19.95	24.92	25.92	25.74	25.67
90	15.72	14.43	14.43	13.30	19.05	20.12	19.94	17.72
110	12.70	11.04	11.04	09.97	15.42	14.50	13.59	12.70

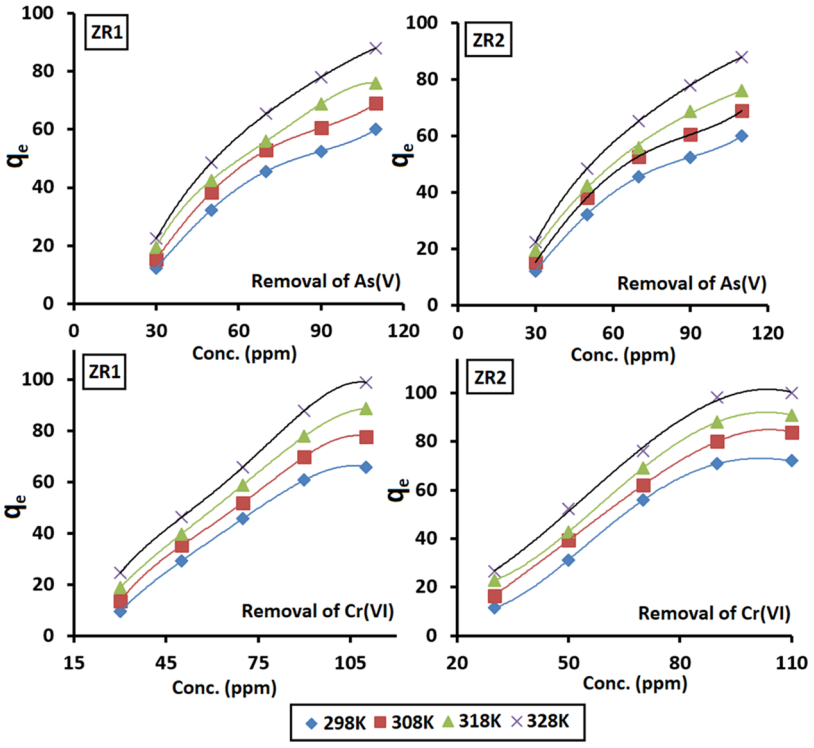

Figure 6. Effect of different temperatures on the removal of various As(V) and Cr(VI) concentrations with **ZR1−ZR2** at pH 6.

enlisted in Table 6, which is indicative of the potential adsorption capacities of **ZR1** and **ZR2**.

3.3.1. Adsorption Isotherms. Langmuir and Freundlich isotherms[36] were applied to present the equilibrium state of As and Cr ion adsorption. The Langmuir isotherm was described by a homogeneous surface with monolayer adsorption without any linkage between adsorbent molecules. Langmuir isotherm constants were calculated by the plot between C_e/q_e and C_e.

$$\frac{C_e}{q_e} = \frac{1}{k_L \times q_m} + \frac{C_e}{q_m} \quad (4)$$

where q_m represents the Langmuir constant, i.e., adsorption maxima or theoretical adsorption capacity. This Langmuir constant adsorption maxima or theoretical adsorption capacity means the amount of the adsorbate adsorbed per unit mass of the adsorbent, i.e., mg/g. As(V) and Cr(VI) adsorption onto the surfaces of **ZR1** and **ZR2** were found to follow the Langmuir isotherm model presented in Figure 8. Langmuir adsorption maxima q_m and the Langmuir constant K_L were calculated from the slope of the plots and the interception of the isotherm and tabulated for As(V) and Cr(VI) removal in Table 7.

The maximum As(V) adsorption capacities (q_m) calculated for **ZR1** and **ZR2** were 13.33 and 9.066 mg/g, respectively, and Langmuir constants (k_L) were found to be −0.158 for **ZR1** and −1.063 for **ZR2** at 298−328 K. The maximum Cr(VI) adsorption capacity (q_m) calculated for **ZR1** and **ZR2** was 13.26 mg/g, and the Langmuir constant (k_L) value was found

https://doi.org/10.1021/acsomega.2c05957
ACS Omega 2023, 8, 2098−2111

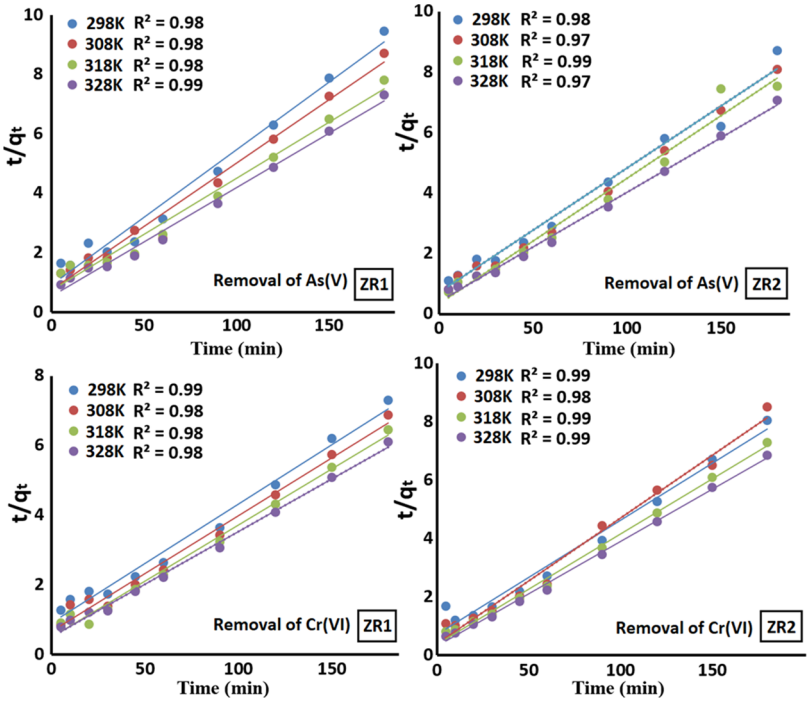

Figure 7. Pseudo-second-order kinetics of the removal of As(V) and Cr(VI) with **ZR1** and **ZR2** at the 298−328 K temperature range and pH 6.

Table 5. Pseudo-Second-Order Kinetic Parameters of the Removal of As(V) and Cr(VI) with ZR1 and ZR2 at the 298−328 K Temperature Range and pH 6

	ZR1			ZR2		
	removal of As(V)					
temperature (K)	R^2	K (min^{-1})	q_e(mg/g)	R^2	K (min^{-1})	q_e(mg/g)
298	0.98	0.00219	22.22	0.98	0.00237	24.33
308	0.98	0.00242	23.47	0.99	0.00309	26.44
318	0.98	0.00142	26.52	0.98	0.00501	24.15
328	0.9912	0.00132	27.47	0.99	0.00313	27.70
	ZR1			**ZR2**		
	removal of Cr(VI)					
temperature (K)	R^2	K (min^{-1})	q_e(mg/g)	R^2	K (min^{-1})	q_e(mg/g)
298	0.99	0.00219	29.23	0.98	0.00224	25.51
308	0.99	0.0017	30.03	0.98	0.00481	23.25
318	0.99	0.0021	30.95	0.99	0.00395	26.45
328	0.99	0.00179	33.00	0.99	0.00356	27. 85

Table 6. Comparison of the Adsorption Capacities of Various Literature-Reported Adsorbents for As(V) and Cr(VI)

metals	adsorbents	adsorption capacity (mg/g)	ref
As(V)	banana peduncle (**ZR1** and **ZR2**)	27.47 and 27.70	this work
	banana trunk	1.04	30
	orange peel	4.27	31
	banana peel	1.35	32
Cr(VI)	banana peduncle (**ZR1** and **ZR2**)	33.00 and 27.85	this work
	modified fly ash	21	33
	orange peel	3.3	34
	banana peel	3.0	35

to be −0.258 for **ZR1** and **ZR2** at 298−328 K. Freundlich isotherms[36] were used to describe adsorption onto a heterogeneous surface. Figure 9 is obtained by plotting log C versus log q_e, and a straight line was obtained showing both As(V) and Cr(VI) adsorption onto **ZR1** and **ZR2**.

$$\ln q_e = \ln q_e + \frac{1}{n} \ln C_e \tag{5}$$

The values of Freundlich constants n and K_F were ascertained from the slope and intercept of the isotherm, as presented in Table 6, for As(V) and Cr(VI), respectively. As and Cr ions were not adsorbed favorably by **ZR1** and **ZR2**, since the n values were less than 1. The nonlinear regression analysis coefficient of determination (R^2) was calculated (Table 7) to examine the fitness of two isotherm models with adsorption isotherm data, which indicated Langmuir as the most fitted isotherm on the experimental data. The mean absolute error (MAE) was calculated for both isotherms by the following equation:

https://doi.org/10.1021/acsomega.2c05957
ACS Omega 2023, 8, 2098−2111

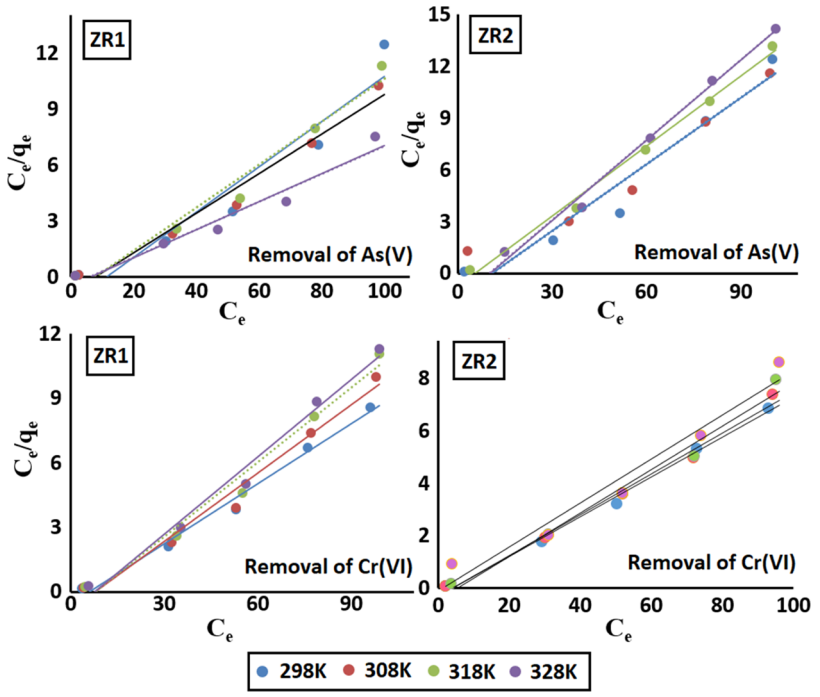

Figure 8. Langmuir isotherms of the % removal of As(V) and Cr(VI) with **ZR1−ZR2** at the 298−328 K temperature range and pH 6.

Table 7. Freundlich and Langmuir Separation Parameters for the Removal of As(V) and Cr(VI) with ZR1−ZR2 at the 298−328 K Temperature Range and pH 6

	removal of As(V)							
	Freundlich isotherm parameters (ZR1)				Langmuir isotherm parameters (ZR1)			
temp. (K)	R^2	n	K_F	MAE	R^2	q_m	K_L	MAE
298	0.83	−3.783	31.42	0.0345	0.92	8.244	−0.088	0.0038
308	0.92	−4.866	27.24	0.0079	0.97	9.442	−0.128	0.1794
318	0.92	−4.926	25.02	0.0083	0.97	8.695	−0.127	0.0012
298	0.73	−4.098	28.94	0.0165	0.96	13.33	−0.158	0.0087
	Freundlich isotherm parameters (ZR2)				Langmuir isotherm parameters (ZR2)			
temp. (K)	R^2	n	K_F	MAE	R^2	q_m	K_L	MAE
298	0.77	−4.241	28.94	0.0215	0.95	7.763	−0.091	0.0321
308	0.97	−3.821	29.50	0.0112	0.95	9.066	−1.063	0.0453
318	0.99	−3.145	31.75	0.0032	0.99	7.369	−0.175	0.0072
328	0.88	−6.207	14.41	0.0213	0.99	6.447	−0.098	0.1657
	removal of Cr(VI)							
	Freundlich isotherm parameters (ZR1)				Langmuir isotherm parameters (ZR1)			
temp. (K)	R^2	n	K_F	MAE	R^2	q_m	K_L	MAE
298	0.96	−5.208	27.59	0.0276	0.99	13.26	−0.258	0.0067
308	0.92	−4.434	29.38	0.0361	0.99	12.87	−0.254	0.0036
318	0.98	−3.829	31.03	0.1769	0.99	12.1	−0.191	0.0104
328	0.99	−3.586	31.8	0.0059	0.96	11.94	−0.771	0.0049
	Freundlich isotherm parameters (ZR2)				Langmuir isotherm parameters (ZR2)			
temp. (K)	R^2	n	K_F	MAE	R^2	q_m	K_L	MAE
298	0.96	−7.855	24.68	0.0087	0.99	13.26	−0.258	0.1391
308	0.97	−7.547	24.42	0.0345	0.99	12.87	−0.254	0.0098
318	0.94	−6.423	25.84	0.0298	0.98	12.10	−0.190	0.0067
328	0.95	−5.599	27.26	0.0093	0.96	11.94	−0.770	0.1462

$$\text{MAE} = \frac{1}{n}\sum_{i=1}^{n}|x_i - x| \quad (6)$$

3.3.2. Thermodynamic Parameters. Thermodynamic parameters such as enthalpy, entropy, and Gibbs free energy[37] have been calculated separately for As(V) and chromium(VI) by **ZR1** and **ZR2** following the standard thermodynamic equations as follows:

$$\Delta G = -RT \ln K_c \quad (7)$$

https://doi.org/10.1021/acsomega.2c05957
ACS Omega 2023, 8, 2098−2111

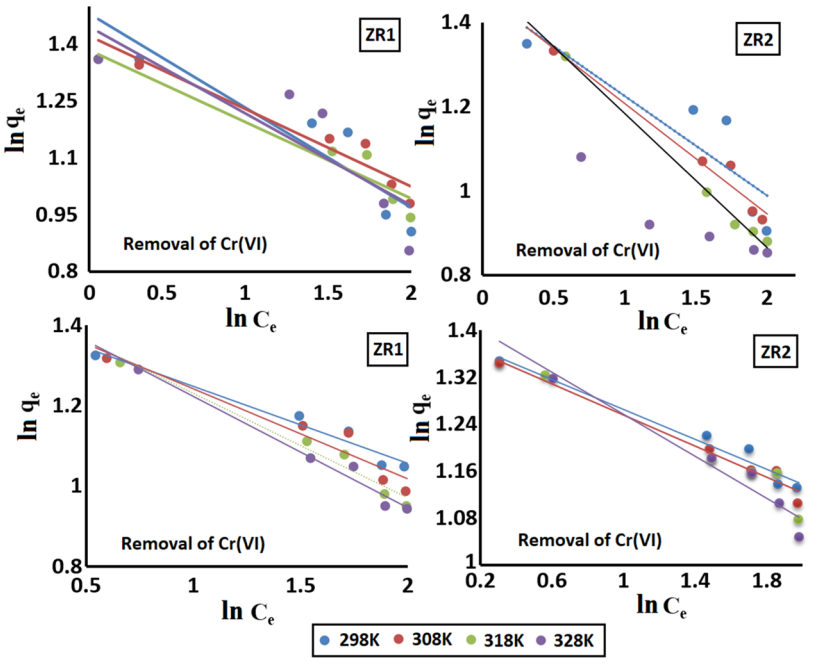

Figure 9. Freundlich isotherm of the removal of As(V) and Cr(VI) with **ZR1**−**ZR2** at the 298−328 K temperature range and pH 6.

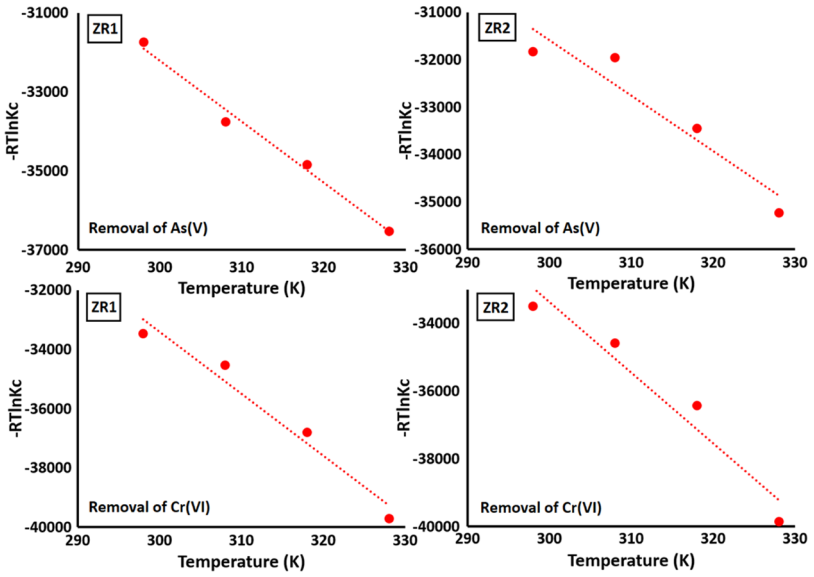

Figure 10. van't Hoff plots for the removal of As(V) and Cr(VI) with **ZR1** and **ZR2**.

Table 8. Enthalpy, Entropy, and Gibbs Free Energy Calculated from van't Hoff Plots for the Removal of As(V) and Cr(VI) with ZR1 and ZR2 at the 298−328 K Temperature Range and pH 6

	removal of As(V)		removal of Cr(VI)	
parameters	**ZR1**	**ZR2**	**ZR1**	**ZR2**
R^2	0.9876	0.9022	0.9396	0.9625
ΔH(kJ/mol)	14138	3557.5	29387	29632
ΔS(kJ/mol·K)	154.49	117.15	209.19	210.08
ΔG(kJ/mol)	-3.17×10^4 (298 K)	-3.18×10^4 (298 K)	-3.35×10^4 (298 K)	-3.35×10^4 (298 K)
	-3.38×10^4 (308 K)	-3.19×10^4 (308 K)	-3.45×10^4 (308 K)	-3.45×10^4 (308 K)
	-3.48×10^4 (318 K)	-3.34×10^4 (318 K)	-3.64×10^4 (318 K)	-3.68×10^4 (318 K)
	-3.65×10^4 (328 K)	-3.52×10^4 (328 K)	-3.99×10^4 (328 K)	-3.97×10^4 (328 K)

$$\Delta G = \Delta H - T\Delta S \quad (8)$$

$$-RT \ln K_c = H - T\Delta S \quad (9)$$

where T is the temperature in "K" and R is the ideal gas constant (8.314 J/mol·K). K_c is the thermodynamic equilibrium constant calculated using eq 9 as follows:

https://doi.org/10.1021/acsomega.2c05957
ACS Omega 2023, 8, 2098−2111

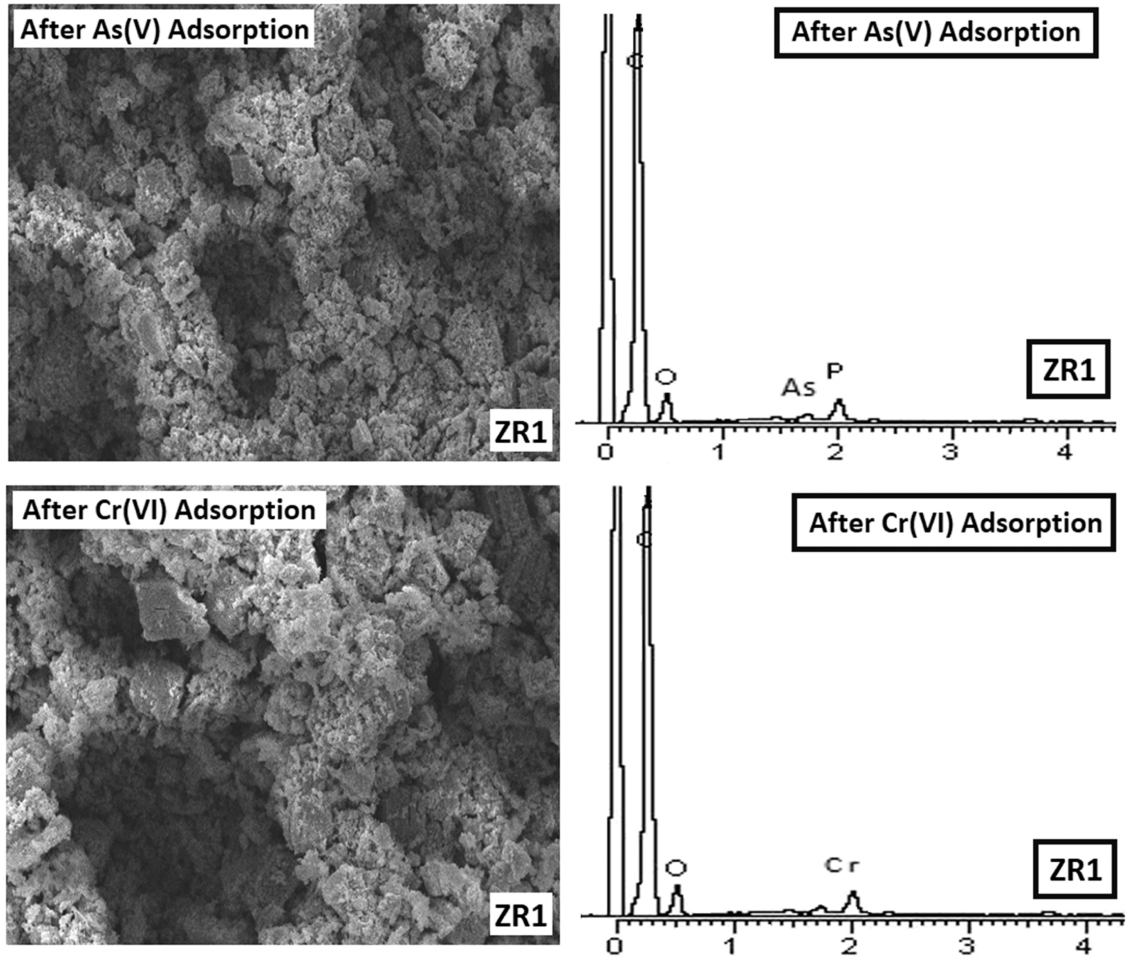

Figure 11. SEM and EDX spectra of **ZR1** after adsorption of As(V) and Cr(VI) activity.

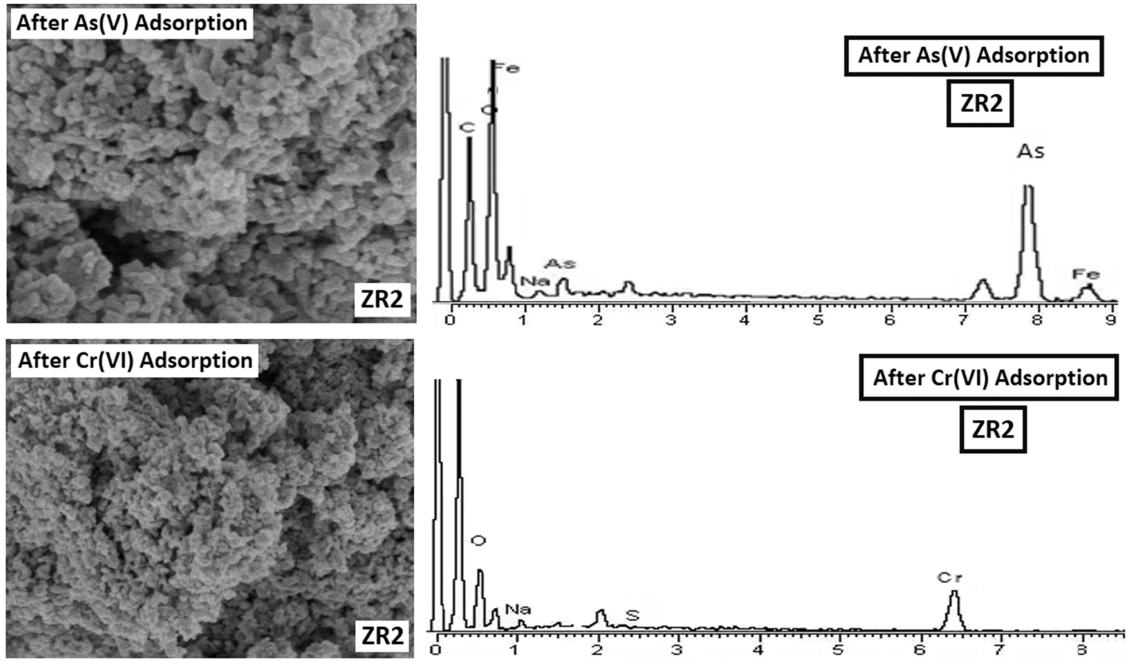

Figure 12. SEM and EDX spectra of **ZR2** after adsorption of As(V) and Cr(VI) activity.

$$K_c = M_w \times 55.5 \times 1000 \times K_L \quad (10)$$

where M_w (g/mol) is the molar mass of the adsorbate (metal ions), K_L (L/mg) is the Langmuir constant, and 55.5 is the

https://doi.org/10.1021/acsomega.2c05957
ACS Omega 2023, 8, 2098−2111

moles of water per liter (1000 g/L divided with 18 g/mol). $\Delta G°$, $\Delta H°$, and $\Delta S°$ are the changes in Gibbs free energy, enthalpy, and entropy, which were determined thermodynamic parameters by plotting $-RT \ln K_c$ versus T, as shown in Figure 10 and enlisted in Table 8. The reaction was spontaneous due to the negative ΔG value and endothermic due to the positive value of ΔH, while ΔS showed increased randomness at the solid/liquid interface. Overall, the banana peduncle was found a potential and best alternative for the removal of Cr(VI) and As(V) from the aqueous phase.

3.4. Desorption Analysis. The reversibility of As(V) and Cr(VI) and chromate anions from the loaded surface of **ZR1** and **ZR2** back into the solution was studied at different pH values (pH 2−10). The results of the desorption of arsenate and chromate at different pH values are presented in Figure S3 in the Supporting Information. It was observed that in the pH range of 2−7, there was no leaching of As(V) and Cr(VI) from **ZR1** and **ZR2** back into the solution. However, in the alkaline region above pH 7, detachment of As(V) and Cr(VI) started from the surface of adsorbents into the solution and reached the maximum desorption of As(V) of 70−60% using **ZR1** and **ZR2** and desorption of Cr(VI) of 76−68% at pH 10. The reason for desorption in the alkaline pH may be due to the increase in OH^- ions, which are responsible for the leaching of As(V) and Cr(VI) from the surface into the aqueous phase.[38] The decrease in equilibrium pH after arsenate and chromate desorption also validates that OH^- ions were consumed for the release of metal ions from the solid surface to the aqueous phase. Desorption analysis indicated that materials are stable structurally and can be efficiently reused for further analysis, which was also confirmed by the characterization of materials after adsorption.

3.5. Characterization of Adsorbents (ZR1−ZR2) after Adsorption Activity. *3.5.1. SEM and EDX Analysis.* SEM and EDX analysis was carried out to evaluate the surface stability and adsorption efficiency of **ZR1** and **ZR2** after the removal activity of As(V) and Cr(VI). SEM micrographs represented no significant change in the surface morphology of the **ZR1** after adsorption, indicating its stability as an adsorbent, whereas EDX analysis of **ZR1** confirmed the presence of As ions, as shown in Figure 11.

The SEM of the **ZR2** sample after adsorption showed more spaces and pores in the cavities, whereas EDX spectra indicated the presence of Cr ions, indicating the efficiency of the adsorbent for removal activities, as shown in Figure 12.

3.5.2. BET Surface Analysis. The BET surface area parameters of activated carbons after adsorption activity with As(V) and Cr(VI) were calculated, and results with representative **ZR1** are enlisted in Tables 9 and 10. Surface areas decreased for the catalysts after adsorption activity. Pore volume for **ZR1** was greater after As(V) adsorption (0.188 cm^3/g) than that after Cr(VI) adsorption (0.266 cm^3/g), which was significantly lowered compared to parameters obtained before activity. This might be attributed to the fact that in the case of an unloaded surface, the adsorbates had not covered the surface area, while in the latter cases, some of the surface areas had been occupied by the adsorbate species. These characters have shown the efficient adsorbent characteristics of activated carbons after the removal of As(V) and Cr(VI).

Table 9. Percentage Desorption of As(V) and Cr(VI) from the Surfaces of ZR1 and ZR2 at Different pH Values at 298 K

	% desorption of As(V)		% desorption of Cr(VI)	
pH	**ZR1**	**ZR2**	**ZR1**	**ZR2**
1	0.00	0.00	0.00	0.00
2	0.00	0.00	0.00	0.00
3	0.00	0.00	0.00	0.00
4	0.00	0.00	0.00	0.00
5	0.00	0.00	0.00	0.00
6	10.01	05.01	15.01	8.02
7	20.02	15.02	25.00	18.01
8	35.02	25.03	40.05	32.00
9	55.05	45.02	60.03	48.00
10	70.00	60.00	76.00	68.00

Table 10. Surface Area Analysis of ZR1 after Adsorption of As(V) and Cr(VI)

properties	**ZR1** with As(V)	**ZR1** with Cr(VI
surface area (S_{BET}), m^2/g	66.12	86.53
surface area (DR), m^2	19.16	31.88
average pore width (DR), (Å)	89.48	109.34
adsorption energy (DR), kJ/mol	0.44	0.68
micropore volume (DR), (cm^3/g)	0.25	0.40
micropore surface area (DR), (m^2/g)	09.88	12.88
pore diameter (DA), (Å)	1.16	1.34
surface area (BJH), (m^2/g)	79.62	91.04
pore volume (BJH), (cm^3/g)	0.188	0.266

4. CONCLUSIONS

ZR1 and **ZR2** have been proven to be potential adsorbents for As(V) and Cr(VI) ion removal. The pH and point of zero charges have been calculated to be 4 and 6, which indicate the acidic nature of Cr(VI) and As(V), respectively. Arsenate and chromate both have greater surface areas and have anionic species, and hence, electrostatic interactions were responsible for the maximum removal of these sorbents from the aquatic environment. At lower pH 4, 100% removal has occurred. Both kinetic models have been applied, while the pseudo-second-order model was the best fitted to the adsorption kinetic data. Both Langmuir and Freundlich models were used to review the temperature effect and to obtain the theoretical adsorption capacities of **ZR1** and **ZR2**. The maximum As(V) adsorption capacities (q_m) calculated for **ZR1** and **ZR2** were 13.33 and 9.066 mg/g, respectively, and Langmuir constants (k_L) were found to be −0.158 for **ZR1** and −1.063 for **ZR2** at 298−328 K. The maximum Cr(VI) adsorption capacity (q_m) calculated for **ZR1** and **ZR2** was 13.26 mg/g, and the Langmuir constant (k_L) was found to be −0.258 for **ZR1** and **ZR2** at 298−328 K. The Langmuir model exposed a good coincidence with thermodynamic data based on regression coefficient R^2 values. The thermodynamic parameters were estimated from the application of the van't Hoff plot and the Gibbs free energy equation. The reaction was spontaneous as ΔG was negative and endothermic as ΔH was positive, and decreased randomness at the solid−liquid interface was shown by ΔS. **ZR1** and **ZR2** were concluded to be efficient and low-cost adsorbents for wastewater treatment in aquatic environments.

https://doi.org/10.1021/acsomega.2c05957
ACS Omega 2023, 8, 2098−2111

■ ASSOCIATED CONTENT

Supporting Information

The Supporting Information is available free of charge at https://pubs.acs.org/doi/10.1021/acsomega.2c05957.

PZC and FTIR spectra and tables incorporating the amounts (q_e) of As(V) and Cr(VI) adsorbed on the surface of catalysts (PDF)

■ AUTHOR INFORMATION

Corresponding Authors

Muhammad Hamayun − *Department of Chemistry, University of Gujrat, Gujrat 50700, Pakistan*; Phone: +92-333-9734401; Email: hamayunf@uog.edu.pk

Ataf Ali Altaf − *Department of Chemistry, University of Okara, Okara 56300, Pakistan*; orcid.org/0000-0001-8018-5890; Phone: +92-332-5049532; Email: atafali_altaf@yahoo.com

Authors

Zobia Razzaq − *Department of Chemistry, University of Gujrat, Gujrat 50700, Pakistan*

Shahzad Murtaza − *Institute of Chemistry, Khwaja Fareed UEIT, Rahim Yar Khan 64200, Pakistan*

Samia Kausar − *Department of Chemistry, University of Gujrat, Gujrat 50700, Pakistan*; orcid.org/0000-0002-0219-2363

Rizwan Ullah Khan − *Department of Chemistry, University of Gujrat, Gujrat 50700, Pakistan*

Tehzeen Javaid − *Department of Chemistry, University of Gujrat, Gujrat 50700, Pakistan*

Complete contact information is available at: https://pubs.acs.org/10.1021/acsomega.2c05957

Notes

The authors declare no competing financial interest.

■ ACKNOWLEDGMENTS

This research was mainly from the PhD thesis of Z.R. The authors would like to gratefully acknowledge the Department of Chemistry, University of Gujrat, Gujrat for providing an instrumental facility.

■ REFERENCES

(1) Mohammed, A. S.; Kapri, A.; Goel, R.Heavy Metal Pollution: Source, Impact, and Remedies. In *Biomanagement of Metal-Contaminated Soils*; Springer, 2011; pp 1−28.

(2) Baker, B. A.; Cassano, V. A.; Murray, C. Arsenic exposure, assessment, toxicity, diagnosis, and management: guidance for occupational and environmental physicians. *J. Occup. Environ. Med.* **2018**, *60*, e634−e639.

(3) Abernathy, C. O.; Thomas, D. J.; Calderon, R. L. Health effects and risk assessment of arsenic. *J. Nutr.* **2003**, *133*, 1536S−1538S.

(4) Zhou, L.; Duan, Y.; Xu, X. Facile preparation of amine-rich polyamidoamine (PAMAM) gel for highly efficient removal of Cr (VI) ions. *Colloids Surf., A* **2019**, *579*, No. 123685.

(5) Kimbrough, D. E.; Cohen, Y.; Winer, A. M.; Creelman, L.; Mabuni, C. A critical assessment of chromium in the environment. *Crit. Rev. Environ. Sci. Technol.* **1999**, *29*, 1−46.

(6) Proctor, D. M.; Suh, M.; Campleman, S. L.; Thompson, C. M. Assessment of the mode of action for hexavalent chromium-induced lung cancer following inhalation exposures. *Toxicology* **2014**, *325*, 160−179.

(7) den Braver-Sewradj, S. P.; van Benthem, J.; Staal, Y. C.; Ezendam, J.; Piersma, A. H.; Hessel, E. V. Occupational exposure to hexavalent chromium. Part II. Hazard assessment of carcinogenic effects. *Regul. Toxicol. Pharmacol.* **2021**, *126*, No. 105045.

(8) Zamora-Ledezma, C.; Negrete-Bolagay, D.; Figueroa, F.; Zamora-Ledezma, E.; Ni, M.; Alexis, F.; Guerrero, V. H. Heavy metal water pollution: A fresh look about hazards, novel and conventional remediation methods. *Environ. Technol. Innov.* **2021**, *22*, No. 101504.

(9) Lakherwal, D. Adsorption of heavy metals: a review. *Int. J. Environ. Res. Dev.* **2014**, *4*, 41−48.

(10) Lim, A. P.; Aris, A. Z. A review on economically adsorbents on heavy metals removal in water and wastewater. *Rev. Environ. Sci. Bio/Technol.* **2014**, *13*, 163−181.

(11) (a) Kheradmand, A.; Negarestani, M.; Mollahosseini, A.; Shayesteh, H.; Farimaniraad, H. Low-cost treated lignocellulosic biomass waste supported with FeCl3/Zn (NO3) 2 for water decolorization. *Sci. Rep.* **2022**, *12*, No. 4497. (b) Burakov, A. E.; Galunin, E. V.; Burakova, I. V.; Kucherova, A. E.; Agarwal, S.; Tkachev, A. G.; Gupta, V. K. Adsorption of heavy metals on conventional and nanostructured materials for wastewater treatment purposes: A review. *Ecotoxicol. Environ. Saf.* **2018**, *148*, 702−712. (c) Kheradmand, A.; Negarestani, M.; Kazemi, S.; Shayesteh, H.; Javanshir, S.; Ghiasinejad, H. Adsorption behavior of rhamnolipid modified magnetic Co/Al layered double hydroxide for the removal of cationic and anionic dyes. *Sci. Rep.* **2022**, *12*, No. 14623. (d) Abadian, S.; Shayesteh, H.; Rahbar-Kelishami, A. Effective adsorption of diclofenac sodium from aqueous solution using cationic surfactant modified Cuminum cyminum agri-waste: Kinetic, equilibrium, and thermodynamic studies. *Int. J. Phytorem.* **2022**, 1−11.

(12) Duan, C.; Ma, T.; Wang, J.; Zhou, Y. Removal of heavy metals from aqueous solution using carbon-based adsorbents: A review. *J. Water Process Eng.* **2020**, *37*, No. 101339.

(13) (a) Tiegam, R. F. T.; Tchuifon, D. R. T.; Santagata, R.; Nanssou, P. A. K.; Anagho, S. G.; Ionel, I.; Ulgiati, S. Production of activated carbon from cocoa pods: Investigating benefits and environmental impacts through analytical chemistry techniques and life cycle assessment. *J. Cleaner Prod.* **2021**, *288*, No. 125464. (b) Tan, J.; Song, Y.; Huang, X.; Zhou, L. Facile functionalization of natural peach gum polysaccharide with multiple amine groups for highly efficient removal of toxic hexavalent chromium (Cr (VI)) ions from water. *ACS Omega* **2018**, *3*, 17309−17318. (c) Zeng, S.; Long, J.; Sun, J.; Wang, G.; Zhou, L. A review on peach gum polysaccharide: Hydrolysis, structure, properties and applications. *Carbohydr. Polym.* **2021**, No. 119015.

(14) Karim, A. A.; Kumar, M.; Mohapatra, S.; Panda, C.; Singh, A. Banana peduncle biochar: characteristics and adsorption of hexavalent chromium from aqueous solution. *Methodology* **2014**, *7*, 1−10.

(15) Arunakumara, K.; Walpola, B. C.; Yoon, M.-H. Banana peel: A green solution for metal removal from contaminated waters. *Korean J. Environ. Agric.* **2013**, *32*, 108−116.

(16) Ceyhan, A. A.; Şahin, Ö.; Baytar, O.; Saka, C. Surface and porous characterization of activated carbon prepared from pyrolysis of biomass by two-stage procedure at low activation temperature and it's the adsorption of iodine. *J. Anal. Appl. Pyrolysis* **2013**, *104*, 378−383.

(17) Hamza, M.; Altaf, A. A.; Kausar, S.; Murtaza, S.; Rasool, N.; Gul, R.; Badshah, A.; Zaheer, M.; Ali Shah, S. A.; Zakaria, Z. A. Catalytic removal of alizarin red using chromium manganese oxide nanorods: degradation and kinetic studies. *Catalysts* **2020**, *10*, 1150.

(18) Aydın, H.; Bulut, Y.; Yerlikaya, Ç. Removal of copper (II) from aqueous solution by adsorption onto low-cost adsorbents. *J. Environ. Manage.* **2008**, *87*, 37−45.

(19) Narasimharao, K.; Lingamdinne, L. P.; Al-Thabaiti, S.; Mokhtar, M.; Alsheshri, A.; Alfaifi, S. Y.; Chang, Y.-Y.; Koduru, J. R. Synthesis and characterization of hexagonal MgFe layered double hydroxide/grapheme oxide nanocomposite for efficient adsorptive removal of cadmium ion from aqueous solutions: Isotherm, kinetic, thermodynamic and mechanism. *J. Water Process Eng.* **2022**, *47*, No. 102746.

(20) Mahmood, T.; Saddique, M. T.; Naeem, A.; Westerhoff, P.; Mustafa, S.; Alum, A. Comparison of different methods for the point

of zero charge determination of NiO. *Ind. Eng. Chem. Res.* **2011**, *50*, 10017−10023.
(21) Kinniburgh, D. G.; Syers, J. K.; Jackson, M. L. Specific adsorption of trace amounts of calcium and strontium by hydrous oxides of iron and aluminum. *Soil Sci. Soc. Am. J.* **1975**, *39*, 464−470.
(22) (a) Gęca, M.; Wiśniewska, M.; Nowicki, P. Biochars and activated carbons as adsorbents of inorganic and organic compounds from multicomponent systems−A review. *Adv. Colloid Interface Sci.* **2022**, *305*, No. 102687. (b) Bello, O. S.; Ahmad, M. A.; Ahmad, N. Adsorptive features of banana (Musa paradisiaca) stalk-based activated carbon for malachite green dye removal. *Chem. Ecol.* **2012**, *28*, 153−167. (c) Ogunleye, O.; Adio, O.; Salawudeen, T. Removal of lead (ii) from aqueous solution using banana (musa paradisiaca) stalk-based activated carbon. *Chem. Process Eng. Res.* **2014**, *28*, 45−59. (d) Nik Yusuf, N. A. A.; Rosly, E. S.; Mohamed, M.; Abu Bakar, M. B.; Yusoff, M.; Sulaiman, M. A.; Ahmad, M. I.*Waste Banana Peel and Its Potentialization in Agricultural Applications: Morphology Overview*; Materials Science Forum, Trans Tech Publ, 2016; pp 394−398.
(23) Girgis, B. S.; Temerk, Y. M.; Gadelrab, M. M.; Abdullah, I. D. X-ray diffraction patterns of activated carbons prepared under various conditions. *Carbon Lett.* **2007**, *8*, 95−100.
(24) Chang, Q.; Lin, W.; Ying, W.-c. Preparation of iron-impregnated granular activated carbon for arsenic removal from drinking water. *J. Hazard. Mater.* **2010**, *184*, 515−522.
(25) Atkinson, J. D.; Fortunato, M. E.; Dastgheib, S. A.; Rostam-Abadi, M.; Rood, M. J.; Suslick, K. S. Synthesis and characterization of iron-impregnated porous carbon spheres prepared by ultrasonic spray pyrolysis. *Carbon* **2011**, *49*, 587−598.
(26) Salman, J.; Njoku, V.; Hameed, B. Adsorption of pesticides from aqueous solution onto banana stalk activated carbon. *Chem. Eng. J.* **2011**, *174*, 41−48.
(27) Ogunleye, O. O.; Ajala, M. A.; Agarry, S. E. Evaluation of biosorptive capacity of banana (Musa paradisiaca) stalk for lead (II) removal from aqueous solution. *J. Environ. Prot.* **2014**, *5*, 1451.
(28) Maji, S. K.; Pal, A.; Pal, T.; Adak, A. Adsorption thermodynamics of arsenic on laterite soil. *J. Surf. Sci. Technol.* **2007**, *22*, 161−176.
(29) Kausar, S.; Altaf, A. A.; Hamayun, M.; Danish, M.; Zubair, M.; Naz, S.; Muhammad, S.; Zaheer, M.; Ullah, S.; Badshah, A. Soft template-based bismuth doped zinc oxide nanocomposites for photocatalytic depolymerization of lignin. *Inorg. Chim. Acta* **2020**, *502*, No. 119390.
(30) Mohd Yasim, N. S. E.; Ismail, Z. S.; Zaki, S. M.; Azis, M. F. A. Adsorption of Cu, As, Pb and Zn by banana trunk. *Malaysian J. Anal. Sci.* **2016**, *20*, 187−196.
(31) Kamsonlain, S.; Balomajumder, C.; Chand, S.*Studies on Surface Characterisation and Isotherm Modelling: Biosorption of Arsenic(III) onto Low Cost Biosorbent Derived from Orange Peel*; NISCAIR-CSIR, 2012.
(32) Kamsonlian, S.; Balomajumder, C.; Chand, S. A potential of biosorbent derived from banana peel for removal of As (III) from contaminated water. *Int. J. Chem. Sci. Appl.* **2012**, *3*, 269−275.
(33) Gupta, S.; Babu, B. In *Adsorption of Chromium (VI) by a Low-Cost Adsorbent Prepared from Tamarind Seeds*, Proceedings of International Symposium & 59th Annual Session of IIChE in Association with International Partners (CHEMCON-2006), GNFC Complex, Bharuch, 2006; pp 27−30.
(34) Castañeda-Figueredo, J. S.; Torralba-Dotor, A. I.; Pérez-Rodríguez, C. C.; Moreno-Bedoya, A. M.; Mosquera-Vivas, C. S. Removal of lead and chromium from solution by organic peels: effect of particle size and bio-adsorbent. *Heliyon* **2022**, *8*, No. e10275.
(35) Ali, A.; Saeed, K.; Mabood, F. Removal of chromium (VI) from aqueous medium using chemically modified banana peels as efficient low-cost adsorbent. *Alexandria Eng. J.* **2016**, *55*, 2933−2942.
(36) Ezzati, R. Derivation of pseudo-first-order, pseudo-second-order and modified pseudo-first-order rate equations from Langmuir and Freundlich isotherms for adsorption. *Chem. Eng. J.* **2020**, *392*, No. 123705.
(37) Lima, E. C.; Hosseini-Bandegharaei, A.; Moreno-Piraján, J. C.; Anastopoulos, I. A critical review of the estimation of the thermodynamic parameters on adsorption equilibria. Wrong use of equilibrium constant in the Van't Hoof equation for calculation of thermodynamic parameters of adsorption. *J. Mol. Liq.* **2019**, *273*, 425−434.
(38) Raichur, A. M.; Panvekar, V. Removal of As(V) by adsorption onto mixed rare earth oxides. *Sep. Sci. Technol.* **2002**, *37*, 1095−1108.

https://doi.org/10.1021/acsomega.2c05957
ACS Omega 2023, 8, 2098−2111